Progress In Electromagnetics Research B, Vol. 44, 405–425, 2012

SMALL TARGET DETECTION IN HEAVY SEA CLUTTER

S. J. Chen*, L. J. Kong, and J. Y. Yang

School of Electronic Engineering, University of Electronic Science and Technology of China, Chengdu, Sichuan 611731, China

Abstract—This paper mainly deals with the detection problem of the target with low Radar Cross-Section (RCS) in heavy sea clutter with unknown Power Spectral Density (PSD). Since the performance of traditional single-scan detectors degrades as the target of interest is smaller and weaker, three adaptive detectors, based upon a two-step design procedure, are proposed within the framework of the multiple-scan signal model. Firstly, the Multiple-Scan Detectors (MSDs) are derived according to the Generalized Likelihood Ratio Test (GLRT), Rao and Wald tests respectively under the assumption that the PSD of primary data is known. Secondly, three strategies are resorted to estimate the unknown PSD, and their Constant False Alarm Rate (CFAR) properties are assessed. Finally, numerical simulation results show that the adaptive MSDs outperform the traditional single-scan detector using Monte Carlo method.

1. INTRODUCTION

Detection for small targets has become a critical application for High Resolution (HR) radar [1–4], specially the buoys, human divers, or small boats in the marine surveillance radar [5]. Since HR reduces the resolution cell size in the scenario illuminated by a radar system, the statistical assumption that the sea clutter is Gaussian or Rayleigh distributed [6, 7] may not be appropriate for the real world. Consequently, for the sake of accurately describing the distribution of the sea clutter to avoid the deterioration of the detection performance in HR radar, numerous research efforts are devoted to both the theoretical modeling of sea backscatter [8–10] and the statistical analysis of the recorded live data of HR sea clutter [11–15].

Received 21 July 2012, Accepted 8 October 2012, Scheduled 8 October 2012

* Corresponding author: Si Jia Chen (sijia.chenee@gmail.com).

The results of both the theoretical and empirical analysis show that HR sea clutter can be modeled as a physically motivated compound-Gaussian process, which can be mathematically described as Spherically Invariant Random Process (SIRP) of the produce of two components, speckle and texture. The speckle component represents the local backscattering, and the texture component denotes the local clutter power fluctuation along the resolution cells. Meanwhile, the experimental evidence indicates that more heavy-tailed clutter models should be considered in HR radar, especially at low grazing angles [16]. In particular, the K-distributed clutter, a kind of compound-Gaussian clutter, has fairly mathematical benefits that other heavy-tailed distributions lack and is thereby popular in the literature [8].

Traditionally, the backscattered energy of large obstacles with high Radar Cross-Section (RCS), such as icebergs or ships, is generally greater than that of sea clutter. Hence, they can be easily detectable given the observational samples corresponding to the output of HR radar system. Conversely, since the target with low RCS is commonly covered by the heavy sea clutter, many conventional single-scan processors, such as the Kelly detector, the Adaptive Matched Filter (AMF) and the Normalized Adaptive Matched Filter (NAMF), suffer serious performance loss and present low detectability. Consequently, in order to improve the detectability for the small target in an oceanic environment, some multiple-scan methods are proposed in the literature. The researchers provide the method of multiple-scan signal averaging to mitigate the effect of noise (not clutter), resulting in the detection performance improvement [17]. The scan-to-scan processors of fast scan rates have been extensively used to suppress approximately Gaussian clutter and detect the radar target of interest [18, 19]. Recently, the detection performance of a multiple-scan application, so-called Radon transform, is tested against the real HR sea clutter [20]. According to these methods, both the empirical results with the real sea clutter and the theoretical counterparts with Gaussian-distributed noise or clutter, ensure that the detectability for the small target can be efficiently improved by using multiple-scan procedures. However, these methods do not concentrate on the theoretical analysis of adaptive multiple-scan detection for a signal of interest under a background of compound-Gaussian clutter.

Therefore, within the multiple-scan framework, the theoretical derivation of optimum, yet nonadaptive Multiple-Scan Detector (MSD) based on Neyman-Pearson (NP) criterion is first proposed. In order to adapt the MSD to unknown clutter covariance matrix, three suboptimum MSDs are then presented. More precisely, the adaptive

MSDs are designed by two-step procedure. In the first step, resorting to the Generalized Likelihood Ratio Test (GLRT), Rao and Wald tests, respectively, the MSDs are derived under the assumption for the known prior information of the clutter, i.e., the Power Spectral Density (PSD), also referred to as the clutter covariance matrix. Obviously, in general conditions, the PSD of the clutter is unknown. Therefore, three methods, i.e., the Sample Covariance Matrix (SCM) estimation, the Normalized Sample Covariance Matrix (NSCM) estimation and the Recursive Maximum Likelihood Estimation (RMLE), are used to estimate the PSD based upon the training data set in the second step. Subsequently, the Constant False Alarm Rate (CFAR) properties of the estimation strategies are thoroughly evaluated under the null hypothesis. Finally, the simulation results, using a comprehensive Monte Carlo method, show that the detection performance of the adaptive MSDs is superior to that of the traditional single-scan detector in the presence of different target types. Meanwhile, the effects of the three estimators on the performance are analyzed under the various scenarios.

The remainder of the paper is organized as follows. Section 2 describes the signal models of the target echo and the compound-Gaussian clutter. The MSDs are introduced in Section 3. In Section 4, numerical simulation results based on Monte Carlo are presented. The conclusions are provided in Sections 5.

2. SIGNAL MODEL

To simplify the signal processing considerations associated with the target migration, the data returned from the small target with low speed appear in the same resolution cell for all pluses. Clearly this assumption is commonly unrealistic under real surveillance operations, but selective alignment techniques can be implemented to achieve the same end [21].

Then, assume that a radar transmits a coherent train of N Coherent Processing Interval (CPI) pulses in a single scan and that the receiver properly demodulates, filters and samples the incoming waveform. The observation vector $\mathbf{z}_{ls} \in C^{N\times 1}$ ($C^{N\times 1}$ denotes the $N \times 1$ dimensional complex vector space), independent between two scans, corresponds to the output of the lth range cell and the sth azimuth cell, given by

$$\mathbf{z}_{ls} = [z_{ls}(1), z_{ls}(2), \ldots, z_{ls}(N)]^T \in C^{N\times 1} \tag{1}$$

where $(\cdot)^T$ denotes the transposition operation. Moreover, the problem of detecting a target, occupied in the l_kth range cell and s_kth azimuth

cell in the kth scan ($k = 1, \ldots, K$), can be formulated in terms of the following binary hypothesis test:

$$H_0 : \mathbf{z}_{l_k s_k} = \mathbf{c}_{l_k s_k}, \quad l_k \in \{1, \ldots, L\}, \quad s_k \in \{1, \ldots, S\}$$
$$H_1 : \begin{cases} \mathbf{z}_{l_k s_k} = a_{l_k s_k} \mathbf{p}_{l_k s_k} + \mathbf{c}_{l_k s_k}, & l_k \in \{1, \ldots, L\}, \quad s_k \in \{1, \ldots, S\} \\ \mathbf{z}_{l_{k_w} s_{k_w}} = \mathbf{c}_{l_{k_w} s_{k_w}}, & \\ l_{k_w} \in \{1, \ldots, L\} \backslash \{l_k\}, & s_{k_w} \in \{1, \ldots, S\} \backslash \{s_k\}, \quad w = 1, \ldots, W \end{cases} \tag{2}$$

where $a_{l_k s_k}$ is the unknown parameter, accounting for the target and the channel propagation effects, and $\mathbf{p}_{l_k s_k}$ indicates the known steering vector while $\mathbf{z}_{l_{k_w} s_{k_w}}$ stands for the observation sample of target free in kth scan and W denotes the number of secondary data. Additionally, $\mathbb{A} \backslash \mathbb{B}$ means the set that contains all those elements of $\mathbb{A}$ that are not in $\mathbb{B}$.

In (2), $\mathbf{c}_{l_k s_k}$ is modeled as a Spherically Invariant Random Vector (SIRV) of the produce of two components: speckle and texture. Precisely, it is represented as

$$\mathbf{c}_{l_k s_k} = \sqrt{\tau_{l_k s_k}} \mathbf{x}_{l_k s_k} \tag{3}$$

where the speckle component $\mathbf{x}_{l_k s_k}$ is a complex, circle, zero mean stationary Gaussian vector, and covariance matrix $\mathbf{M}$ is assumed the same for every scan:

$$\mathbf{M} = E\left[\mathbf{x}_{l_k s_k} \mathbf{x}_{l_k s_k}^H\right] \tag{4}$$

where $(\cdot)^H$ denotes the complex conjugate transpose operation, and $E[\cdot]$ is the statistical expectation. The texture component $\tau_{l_k s_k}$ is a nonnegative real random variable with the Probability Density Function (PDF) $p_{\tau_{l_k s_k}}(\tau_{l_k s_k})$.

Given $\tau_{l_k s_k}$, a conditional covariance matrix of $\mathbf{c}_{l_k s_k}$ denotes

$$\mathbf{M}_{l_k s_k | \tau_{l_k s_k}} = E\left[\mathbf{c}_{l_k s_k} \mathbf{c}_{l_k s_k}^H | \tau_{l_k s_k}\right] = \tau_{l_k s_k} \mathbf{M} \tag{5}$$

Under H_0, the PDF of $\mathbf{z}_{l_k s_k}$ can be expressed as

$$\begin{aligned} p\left(\mathbf{z}_{l_k s_k} | \mathbf{M}; H_0\right) &= \frac{1}{\pi^N \|\mathbf{M}\|} h_N\left(q_0(\mathbf{z}_{l_k s_k})\right) \\ &= \frac{1}{\pi^N \|\mathbf{M}\|} \int_0^\infty \tau_{l_k s_k}^{-N} \exp\left(-\frac{q_0(\mathbf{z}_{l_k s_k})}{\tau_{l_k s_k}}\right) p_{\tau_{l_k s_k}}(\tau_{l_k s_k}) \mathrm{d}\tau_{l_k s_k} \end{aligned} \tag{6}$$

with

$$q_0(\mathbf{z}_{l_k s_k}) = \mathbf{z}_{l_k s_k}^H \mathbf{M}^{-1} \mathbf{z}_{l_k s_k} \tag{7}$$

where $\|\cdot\|$ denotes the determinant of a square matrix.

And under H_1, the PDF of $\mathbf{z}_{l_k s_k}$ can be written as

$$p(\mathbf{z}_{l_k s_k}|a_{l_k s_k},\mathbf{M};H_1)=\frac{1}{\pi^N\|\mathbf{M}\|}h_N\left(q_1(\mathbf{z}_{l_k s_k})\right)$$
$$=\frac{1}{\pi^N\|\mathbf{M}\|}\int_0^\infty \tau_{l_k s_k}^{-N}\exp\left(-\frac{q_1(\mathbf{z}_{l_k s_k})}{\tau_{l_k s_k}}\right)p_{\tau_{l_k s_k}}(\tau_{l_k s_k})\mathrm{d}\tau_{l_k s_k} \quad (8)$$

with

$$q_1(\mathbf{z}_{l_k s_k}) = (\mathbf{z}_{l_k s_k} - a_{l_k s_k}\mathbf{p}_{l_k s_k})^H \mathbf{M}^{-1} (\mathbf{z}_{l_k s_k} - a_{l_k s_k}\mathbf{p}_{l_k s_k}) \quad (9)$$

In the slow scan HR radar typically operating with scan rates of about 6–60 rpm, the independence of data is commonly considered between kth scan and $(k+1)$th scan [19], and thereby the joint PDFs of K scans under H_0 and H_1 are:

$$p(\mathbf{z}_{l_1 s_1:l_K s_K}|\mathbf{M};H_0)$$
$$=\frac{1}{\pi^{KN}\|\mathbf{M}\|^K}\prod_{k=1}^K\int_0^\infty \tau_{l_k s_k}^{-N}\exp\left(-\frac{q_0(\mathbf{z}_{l_k s_k})}{\tau_{l_k s_k}}\right)\cdot p_{\tau_{l_k s_k}}(\tau_{l_k s_k})\,\mathrm{d}\tau_{l_k s_k} \quad (10)$$

and

$$p(\mathbf{z}_{l_1 s_1:l_K s_K}|a_{l_1 s_1:l_K s_K},\mathbf{M};H_1)$$
$$=\frac{1}{\pi^{KN}\|\mathbf{M}\|^K}\prod_{k=1}^K\int_0^\infty \tau_{l_k s_k}^{-N}\exp\left(-\frac{q_1(\mathbf{z}_{l_k s_k})}{\tau_{l_k s_k}}\right)p_{\tau_{l_k s_k}}(\tau_{l_k s_k})\,\mathrm{d}\tau_{l_k s_k} \quad (11)$$

3. MULTIPLE-SCAN DETECTORS

According to the NP criterion, the optimum detector is the Likelihood Ratio Test (LRT):

$$\Lambda_{NP}(\mathbf{z}_{l_1 s_1:l_K s_K})=\frac{p(\mathbf{z}_{l_1 s_1:l_K s_K}|a_{l_1 s_1:l_K s_K},\mathbf{M};H_1)}{p(\mathbf{z}_{l_1 s_1:l_K s_K}|\mathbf{M};H_0)}$$
$$=\prod_{k=1}^K\frac{\int_0^\infty \tau_{l_k s_k}^{-N}\exp\left(-\frac{q_1(\mathbf{z}_{l_k s_k})}{\tau_{l_k s_k}}\right)p_{\tau_{l_k s_k}}(\tau_{l_k s_k})\mathrm{d}\tau_{l_k s_k}}{\int_0^\infty \tau_{l_k s_k}^{-N}\exp\left(-\frac{q_0(\mathbf{z}_{l_k s_k})}{\tau_{l_k s_k}}\right)p_{\tau_{l_k s_k}}(\tau_{l_k s_k})\mathrm{d}\tau_{l_k s_k}}\underset{H_0}{\overset{H_1}{\gtrless}}\gamma_{NP} \quad (12)$$

where γ_{NP} is the detection threshold to be set according to the desired value of the probability of false-alarm (P_{fa}).

In many real scenarios, the prior information of $\tau_{l_k s_k}$, $a_{l_k s_k}$ or $\mathbf{M}$ is hardly known, and the NP detector needs a heavy computational integration in test (12). The references [21, 22] show that it is difficult

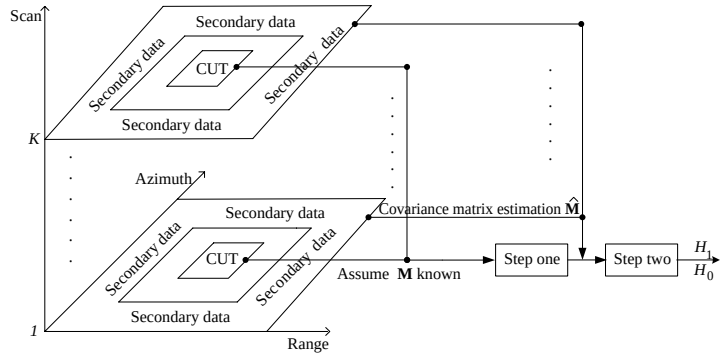

Figure 1. Block diagram of the two-step design procedure.

to jointly maximize with respect to $a_{l_k s_k}$ and unknown $\mathbf{M}$, and a closed-form solution is nonexistent. In order to overcome the drawback, three adaptive MSDs are proposed, resorting to the following two-step design procedure. Firstly, we derive the MSD based upon the GLRT [23, 24], Rao test [25, 26] or Wald test [27] assuming that the structure of covariance matrix is known. Then, the true covariance matrix is substituted by its estimate based upon three suitable estimation methods using the secondary data. Figure 1 illustrates the process of two-step design procedure.

3.1. Step One: Known M

GLRT: The detection algorithm, based upon the primary data, is tantamount to the following decision rule, shown as

$$\begin{aligned}
&\Lambda_{GLRT}(\mathbf{z}_{l_1 s_1:l_K s_K}) \\
=&\frac{\max\limits_{a_{l_1 s_1:l_K s_K}} \left(p(\mathbf{z}_{l_1 s_1:l_K s_K} | a_{l_1 s_1:l_K s_K}; H_1) \right)}{p(\mathbf{z}_{l_1 s_1:l_K s_K} | H_0)} \\
=&\frac{\max\limits_{a_{l_1 s_1:l_K s_K}} \left(\prod\limits_{k=1}^{K} \int_0^{\infty} \tau_{l_k s_k}^{-N} \exp\left(-\frac{q_1(\mathbf{z}_{l_k s_k})}{\tau_{l_k s_k}} \right) p_{l_k s_k}(\tau_{l_k s_k}) \mathrm{d}\tau_{l_k s_k} \right)}{\prod_{k=1}^{K} \int_0^{\infty} \tau_{l_k s_k}^{-N} \exp\left(-\frac{q_0(\mathbf{z}_{l_k s_k})}{\tau_{l_k s_k}} \right) p_{l_k s_k}(\tau_{l_k s_k}) \mathrm{d}\tau_{l_k s_k}} \underset{H_0}{\overset{H_1}{\gtrless}} \gamma_{GLRT}
\end{aligned} \tag{13}$$

where γ_{GLRT} is the threshold, setting with respect to the desired probability of false-alarm.

Generally, further developments of the detector (13) require the specifying $p_{\tau_{l_k s_k}}(\tau_{l_k s_k})$. K-distributed clutter with the modulating

variate $\tau_{l_k s_k}$, as the most popular model for compound-Gaussian clutter, is taken into account in this paper for two reasons: physical plausibility and mathematical convenience, while the PDF of $\tau_{l_k s_k}$, $p_{\tau_{l_k s_k}}(\tau_{l_k s_k})$, is a Gamma distribution, is expressed as

$$p_{\tau_{l_k s_k}}(\tau_{l_k s_k}) = \frac{1}{\Gamma(\nu)} \left(\frac{\nu}{\mu}\right)^{\nu} \tau_{l_k s_k}^{\nu-1} \exp\left(-\frac{\nu}{\mu}\tau_{l_k s_k}\right) \tag{14}$$

where μ determines the mean of the distribution, and the shape parameter ν controls the derivation from the Rayleigh distribution [12, 28] with $\mu = \sqrt{2\nu}$ guaranteeing the unit power of the complex K-distributed clutter in each cell, and Eulerian Gamma function $\Gamma(\cdot)$. In this paper, the two parameters are assumed to be known, and they can also be obtained in terms of the statistical moments as well as goodness-of-fit tests [29].

Then the PDF of $\mathbf{z}_{l_k s_k}$ under the condition of H_0 leads to

$$\begin{aligned} p(\mathbf{z}_{l_1 s_1 : l_K s_K} | H_0) \;=\; & \frac{1}{2^{-K}\Gamma^K(\nu)} \left(\frac{\nu}{\mu}\right)^{\frac{K(\nu+N)}{2}} \\ & \prod_{k=1}^{K} q_0^{\frac{\nu-N}{2}}(\mathbf{z}_{l_k s_k}) K_{\nu-N}\left(\sqrt{4\nu \frac{q_0(\mathbf{z}_{l_k s_k})}{\mu}}\right) \end{aligned} \tag{15}$$

Similarly, the PDF of $\mathbf{z}_{l_k s_k}$ under the condition of H_1 yields

$$\begin{aligned} & p(\mathbf{z}_{l_1 s_1 : l_K s_K} | a_{l_k s_k}; H_1) \\ = & \frac{1}{2^{-K}\Gamma^K(\nu)} \left(\frac{\nu}{\mu}\right)^{\frac{K(\nu+N)}{2}} \prod_{k=1}^{K} q_1^{\frac{\nu-N}{2}}(\mathbf{z}_{l_k s_k}) K_{\nu-N}\left(\sqrt{4\nu \frac{q_1(\mathbf{z}_{l_k s_k})}{\mu}}\right) \end{aligned} \tag{16}$$

with the modified second-kind Bessel function $K_b(\cdot)$ of order b.

Therefore, the test (13) can be rewritten as

$$\begin{aligned} & \Lambda_{GLRT}\left(\mathbf{z}_{l_1 s_1 : l_K s_K}\right) \\ = & \frac{\max\limits_{a_{l_1 s_1 : l_K s_K}} \left(\prod\limits_{k=1}^{K} q_1^{\frac{\nu-N}{2}}(\mathbf{z}_{l_k s_k}) K_{N-\nu}\left(\sqrt{4\nu \frac{q_1(\mathbf{z}_{l_k s_k})}{\mu}}\right)\right)}{\prod_{k=1}^{K} q_0^{\frac{\nu-N}{2}}(\mathbf{z}_{l_k s_k}) K_{N-\nu}\left(\sqrt{4\nu \frac{q_0(\mathbf{z}_{l_k s_k})}{\mu}}\right)} \underset{H_0}{\overset{H_1}{\gtrless}} \gamma_{GLRT} \end{aligned} \tag{17}$$

And the Maximum Likelihood Estimation (MLE) of $a_{l_k s_k}$ is

$$\hat{a}_{l_k s_k} = \frac{\mathbf{p}_{l_k s_k}^H \mathbf{M}^{-1} \mathbf{z}_{l_k s_k}}{\mathbf{p}_{l_k s_k}^H \mathbf{M}^{-1} \mathbf{p}_{l_k s_k}} \tag{18}$$

Substitute $\hat{a}_{l_k s_k}$ into the test (17), then, it is reduced to

$$\Lambda_{GLRT}\left(\mathbf{z}_{l_1 s_1:l_K s_K}\right)=\prod_{k=1}^{K}\left(\frac{\hat{q}_1^{\frac{\nu-N}{2}}\left(\mathbf{z}_{l_k s_k}\right)K_{N-\nu}\left(\sqrt{4\nu\frac{\hat{q}_1\left(\mathbf{z}_{l_k s_k}\right)}{\mu}}\right)}{q_0^{\frac{\nu-N}{2}}\left(\mathbf{z}_{l_k s_k}\right)K_{N-\nu}\left(\sqrt{4\nu\frac{q_0\left(\mathbf{z}_{l_k s_k}\right)}{\mu}}\right)}\right)\underset{H_0}{\overset{H_1}{\gtrless}}\gamma_{GLRT} \quad (19)$$

with

$$\begin{aligned}\hat{q}_1\left(\mathbf{z}_{l_k s_k}\right)&=\left(\mathbf{z}_{l_k s_k}-\hat{a}_{l_k s_k}\mathbf{p}_{l_k s_k}\right)^H\mathbf{M}^{-1}\left(\mathbf{z}_{l_k s_k}-\hat{a}_{l_k s_k}\mathbf{p}_{l_k s_k}\right)\\&=\mathbf{z}_{l_k s_k}^H\mathbf{M}^{-1}\mathbf{z}_{l_k s_k}-\frac{|\mathbf{p}_{l_k s_k}^H\mathbf{M}^{-1}\mathbf{z}_{l_k s_k}|^2}{\mathbf{p}_{l_k s_k}^H\mathbf{M}^{-1}\mathbf{p}_{l_k s_k}}\end{aligned} \quad (20)$$

while $|\cdot|$ denotes the modulus of a complex number.

According to [30], we model the texture as unknown deterministic parameter in the Rao and Wald tests. Then the joint PDFs under H_0 and H_1 are:

$$p(\mathbf{z}_{l_1 s_1:l_K s_K}|\tau_{l_1 s_1:l_K s_K};H_0)=\frac{1}{\pi^{KN}\|\mathbf{M}\|^K}\prod_{k=1}^{K}\frac{1}{\tau_{l_k s_k}^N}\exp\left(\frac{q_0\left(\mathbf{z}_{l_k s_k}\right)}{\tau_{l_k s_k}}\right) \quad (21)$$

and

$$\begin{aligned}&p\left(\mathbf{z}_{l_1 s_1:l_K s_K}|a_{l_1 s_1:l_K s_K},\tau_{l_1 s_1:l_K s_K};H_1\right)\\&=\frac{1}{\pi^{KN}\|\mathbf{M}\|^K}\prod_{k=1}^{K}\frac{1}{\tau_{l_k s_k}^N}\exp\left(\frac{q_1(\mathbf{z}_{l_k s_k})}{\tau_{l_k s_k}}\right)\end{aligned} \quad (22)$$

Rao test: Starting from the primary data and assuming the known $\mathbf{M}$, the detection algorithm implementing the Rao test can be obtained expanding the likelihood ratio in the neighborhood of the MLEs of parameters.

In order to evaluate the decision statistic, we denote with

- $a_{l_k s_k,R}$ and $a_{l_k s_k,I}$ are the real and the imaginary parts of $a_{l_k s_k}, k = 1,\ldots,K$, respectively;
- $\theta_r = [a_{l_1 s_1,R}, a_{l_1 s_1,I},\ldots,a_{l_K s_K,R}, a_{l_K s_K,I}]^T$ a $2K$-dimensional real vector;
- $\theta_u = [\tau_{l_1 s_1},..,\tau_{l_K s_K}]^T$ a K-dimensional real column vector of nuisance parameters;
- $\theta = [\theta_r^T, \theta_u^T]^T$ a $3K$-dimensional real vector.

Therefore, the Rao test for the problem of interest is the following decision rule:

$$\Lambda_{Rao}\left(\mathbf{z}_{l_1 s_1:l_K s_K}\right) = \frac{\partial \ln p(\mathbf{z}_{l_1 s_1:l_K s_K}|\theta)}{\partial \theta_r}\bigg|_{\theta=\hat{\theta}_0}^{T} \left[\mathbf{I}^{-1}\left(\hat{\theta}_0\right)\right]_{\theta_r,\theta_r} \frac{\partial \ln p\left(\mathbf{z}_{l_1 s_1:l_K s_K}|\theta\right)}{\partial \theta_r}\bigg|_{\theta=\hat{\theta}_0} \underset{H_0}{\overset{H_1}{\gtrless}} \gamma_{Rao} \quad (23)$$

where

- γ_{Rao} is the detection threshold to be set with respect to the desired value of the probability of false-alarm;
- $p(\mathbf{z}_{l_1 s_1:l_K s_K}|\theta)$ denotes the PDF of the data under H_1;
- $\partial\theta_r = [\frac{\partial}{\partial a_{l_1 s_1,R}}, \frac{\partial}{\partial a_{l_1 s_1,I}}, \ldots, \frac{\partial}{\partial a_{l_K s_K,R}}, \frac{\partial}{\partial a_{l_K s_K,I}}]^T$ denotes the gradient operator with respect to θ_r;
- $\hat{\theta}_0 = [\theta_{r,0}^T, \hat{\theta}_{u,0}^T]^T$, where $\theta_{r,0}^T = [0, \ldots, 0]^T$ and $\hat{\theta}_{u,0}$ is the MLE of θ_u under H_0;
- $\mathbf{I}(\theta) = \mathbf{I}(\theta_r, \theta_u)$ is the Fisher Information Matrix (FIM) [24], which can be partitioned as

$$\mathbf{I}(\theta) = \begin{bmatrix} \mathbf{I}_{\theta_r,\theta_r}(\theta) & \mathbf{I}_{\theta_r,\theta_u}(\theta) \\ \mathbf{I}_{\theta_u,\theta_r}(\theta) & \mathbf{I}_{\theta_u,\theta_u}(\theta) \end{bmatrix} \quad (24)$$

- $\mathbf{I}^{-1}(\theta)_{\theta_r,\theta_r} = \left(\mathbf{I}_{\theta_r,\theta_r}(\theta) - \mathbf{I}_{\theta_r,\theta_u}\mathbf{I}_{\theta_u,\theta_u}(\theta)\mathbf{I}_{\theta_u,\theta_r}(\theta)\right)^{-1}$.

Hence, according to the Rao test rule, $\hat{\theta}_{u,0}$ can be easily obtained as

$$\hat{\theta}_{u,0} = \frac{1}{N}[q_0(\mathbf{z}_{l_1 s_1}), q_0(\mathbf{z}_{l_2 s_2}), \ldots, q_0(\mathbf{z}_{l_K s_K})]^T \quad (25)$$

Moreover,

$$\frac{\partial \ln p(\mathbf{z}_{l_1 s_1:l_K s_K}|\theta)}{\partial a_{l_k s_k,R}} = 2\mathrm{Re}\left(\frac{\mathbf{p}_{l_k s_k}^H \mathbf{M}^{-1}(\mathbf{z}_{l_k s_k} - a_{l_k s_k}\mathbf{p}_{l_k s_k})}{\tau_{l_k s_k}}\right) \quad (26)$$

$$\frac{\partial \ln p(\mathbf{z}_{l_1 s_1:l_K s_K}|\theta)}{\partial a_{l_k s_k,I}} = 2\mathrm{Im}\left(\frac{\mathbf{p}_{l_k s_k}^H \mathbf{M}^{-1}(\mathbf{z}_{l_k s_k} - a_{l_k s_k}\mathbf{p}_{l_k s_k})}{\tau_{l_k s_k}}\right) \quad (27)$$

where $\mathrm{Re}(\cdot)$ and $\mathrm{Im}(\cdot)$ are the real and the imaginary part of the argument, respectively.

Considering $\theta_{r,0}^T = [0, \ldots, 0]^T$, therefore,

$$\begin{aligned}
&\frac{\partial \ln p(\mathbf{z}_{l_1 s_1 : l_K s_K} | \theta)}{\partial \theta_r}\Big|_{\theta=\hat{\theta}_0}^T \\
&= 2\left[\mathrm{Re}\left(\frac{\mathbf{p}_{l_1 s_1}^H \mathbf{M}^{-1} \mathbf{z}_{l_1 s_1}}{\tau_{l_1 s_1}}\right), \mathrm{Im}\left(\frac{\mathbf{p}_{l_1 s_1}^H \mathbf{M}^{-1} \mathbf{z}_{l_1 s_1}}{\tau_{l_1 s_1}}\right),\right. \\
&\left.\ldots, \mathrm{Re}\left(\frac{\mathbf{p}_{l_K s_K}^H \mathbf{M}^{-1} \mathbf{z}_{l_K s_K}}{\tau_{l_K s_K}}\right), \mathrm{Im}\left(\frac{\mathbf{p}_{l_K s_K}^H \mathbf{M}^{-1} \mathbf{z}_{l_K s_K}}{\tau_{l_K s_K}}\right)\right] \quad (28)
\end{aligned}$$

Further developments require evaluating the blocks of FIM. Then, it can be shown that

$$\begin{aligned}
\mathbf{I}_{\theta_r, \theta_r}(\theta) = 2\mathrm{diag}&\left(\frac{\mathbf{p}_{l_1 s_1}^H \mathbf{M}^{-1} \mathbf{p}_{l_1 s_1}}{\tau_{l_1 s_1}}, \frac{\mathbf{p}_{l_1 s_1}^H \mathbf{M}^{-1} \mathbf{p}_{l_1 s_1}}{\tau_{l_1 s_1}},\right. \\
&\left.\ldots, \frac{\mathbf{p}_{l_K s_K}^H \mathbf{M}^{-1} \mathbf{p}_{l_K s_K}}{\tau_{l_K s_K}}, \frac{\mathbf{p}_{l_K s_K}^H \mathbf{M}^{-1} \mathbf{p}_{l_K s_K}}{\tau_{l_K s_K}}\right) \quad (29)
\end{aligned}$$

and

$$\mathbf{I}_{\theta_r, \theta_u}(\theta) = 0_{2K,K} \quad (30)$$

where $0_{2K,K}$ is a $2K \times K$ matrix of zeros and $\mathrm{diag}(\cdot)$ denotes the diagonal matrix.

As a consequence, plugging (25), (28), (29), (30) into (23), after some algebra, yields

$$\Lambda_{Rao}(\mathbf{z}_{l_1 s_1 : l_K s_K}) = N \sum_{k=1}^{K} \frac{|\mathbf{p}_{l_k s_k}^H \mathbf{M}^{-1} \mathbf{z}_{l_k s_k}|^2}{\mathbf{p}_{l_k s_k}^H \mathbf{M}^{-1} \mathbf{p}_{l_k s_k} \mathbf{z}_{l_k s_k}^H \mathbf{M}^{-1} \mathbf{z}_{l_k s_k}} \underset{H_0}{\overset{H_1}{\gtrless}} \gamma_{Rao} \quad (31)$$

Wald test: The Wald test, based on the primary data, can be obtained exploiting the asymptotic efficiency of the MLE. Precisely, its decision rule denotes

$$\Lambda_{Wald}(\mathbf{z}_{l_1 s_1 : l_K s_K}) = \hat{\theta}_{r,1}^T \left([\mathbf{I}^{-1}(\hat{\theta}_1)]_{\theta_r, \theta_r}\right)^{-1} \hat{\theta}_{r,1} \underset{H_0}{\overset{H_1}{\gtrless}} \gamma_{wald} \quad (32)$$

where

- γ_{wald} is the detection threshold to be set with respect to the desired value of the probability of false-alarm;
- $\hat{\theta}_1 = [\hat{\theta}_{r,1}^T, \hat{\theta}_{u,1}^T]^T$ is the MLE of θ under H_1, i.e.,

$$\hat{\theta}_1 = \mathrm{argmax}_{\theta_1}\left(\frac{1}{\pi^{KN}\|\mathbf{M}\|^K} \prod_{k=1}^{K} \frac{1}{\tau_{l_k s_k}^N} \exp\left(\frac{q_1(\mathbf{z}_{l_k s_k})}{\tau_{l_k s_k}}\right)\right) \quad (33)$$

Maximizing the expression (33) yields

$$\hat{\theta}_{r,1} = \left[\mathrm{Re}\left(\frac{\mathbf{p}_{l_1 s_1}^H \mathbf{M}^{-1} \mathbf{z}_{l_1 s_1}}{\mathbf{p}_{l_1 s_1}^H \mathbf{M}^{-1} \mathbf{p}_{l_1 s_1}} \right), \mathrm{Im}\left(\frac{\mathbf{p}_{l_1 s_1}^H \mathbf{M}^{-1} \mathbf{z}_{l_1 s_1}}{\mathbf{p}_{l_1 s_1}^H \mathbf{M}^{-1} \mathbf{p}_{l_1 s_1}} \right), \ldots, \mathrm{Re}\left(\frac{\mathbf{p}_{l_K s_K}^H \mathbf{M}^{-1} \mathbf{z}_{l_K s_K}}{\mathbf{p}_{l_K s_K}^H \mathbf{M}^{-1} \mathbf{p}_{l_K s_K}} \right), \mathrm{Im}\left(\frac{\mathbf{p}_{l_K s_K}^H \mathbf{M}^{-1} \mathbf{z}_{l_K s_K}}{\mathbf{p}_{l_K s_K}^H \mathbf{M}^{-1} \mathbf{p}_{l_K s_K}} \right) \right]^T \quad (34)$$

and

$$\hat{\theta}_{u,1} = \frac{1}{N} \left[\mathbf{z}_{l_1 s_1}^H \mathbf{M}^{-1} \mathbf{z}_{l_1 s_1} - \frac{|\mathbf{p}_{l_1 s_1}^H \mathbf{M}^{-1} \mathbf{z}_{l_1 s_1}|^2}{\mathbf{p}_{l_1 s_1}^H \mathbf{M}^{-1} \mathbf{p}_{l_1 s_1}}, \ldots, \mathbf{z}_{l_K s_K}^H \mathbf{M}^{-1} \mathbf{z}_{l_K s_K} - \frac{|\mathbf{p}_{l_K s_K}^H \mathbf{M}^{-1} \mathbf{z}_{l_K s_K}|^2}{\mathbf{p}_{l_K s_K}^H \mathbf{M}^{-1} \mathbf{p}_{l_K s_K}} \right]^T \quad (35)$$

Hence, substituting (29), (34) and (35) into (32), we can get

$$\Lambda_{Wald}(\mathbf{z}_{l_1 s_1 : l_K s_K}) = N \sum_{k=1}^{K} \frac{|\mathbf{p}_{l_k s_k}^H \mathbf{M}^{-1} \mathbf{z}_{l_k s_k}|^2}{\mathbf{p}_{l_k s_k}^H \mathbf{M}^{-1} \mathbf{p}_{l_k s_k} \mathbf{z}_{l_k s_k}^H \mathbf{M}^{-1} \mathbf{z}_{l_k s_k} - |\mathbf{p}_{l_k s_k}^H \mathbf{M}^{-1} \mathbf{z}_{l_k s_k}|^2} \underset{H_0}{\overset{H_1}{\gtrless}} \gamma_{wald} \quad (36)$$

In general, the GLRT, Rao and Wald tests have the same asymptotic performance. However, the Rao test does not require evaluating the MLEs of the unknown parameters under H_1 hypothesis, leaving only the MLEs under H_0 to be found, and the Wald test only adopts the data components orthogonal to the useful signal subspace. Therefore, the Rao and Wald tests might require a lower computational complexity than the GLRT for their implementation.

3.2. Step Two: Estimation of M

In order to adapt the MSDs fully to the covariance matrix of clutter, several covariance matrix estimations substitute $\mathbf{M}$ in the tests (19), (31) and (36), respectively.

Herein, the simple and widely method used in Gaussian environment is SCM. In the kth scan, it is shown as

$$\hat{\mathbf{M}}_{SCM_k} = \frac{1}{W} \sum_{w=1}^{W} \mathbf{z}_{l_{k_w} s_{k_w}} \mathbf{z}_{l_{k_w} s_{k_w}}^H \quad (37)$$

When in non-Gaussian clutter scenarios, the NSCM method in the kth scan is commonly applied and written as

$$\hat{\mathbf{M}}_{NSCM_k} = \frac{N}{W} \sum_{w=1}^{W} \frac{\mathbf{z}_{l_{k_w} s_{k_w}} \mathbf{z}_{l_{k_w} s_{k_w}}^H}{\mathbf{z}_{l_{k_w} s_{k_w}}^H \mathbf{z}_{l_{k_w} s_{k_w}}} \quad (38)$$

The NSCM eliminates the effect of the data-dependent normalization factor $\tau_{l_{k_w}s_{k_w}} = \mathbf{z}^H_{l_{k_w}s_{k_w}}\mathbf{z}_{l_{k_w}s_{k_w}}$ accounted for the random local power change from cell to cell.

The third estimation method is called RMLE, in the kth scan, which is

$$\hat{\mathbf{M}}_{RMLE_k}(t)=\frac{N}{W}\sum_{w=1}^{W}\frac{\mathbf{z}_{l_{k_w}s_{k_w}}\mathbf{z}^H_{l_{k_w}s_{k_w}}}{\mathbf{z}^H_{l_{k_w}s_{k_w}}\hat{\mathbf{M}}_{RMLE_k}(t-1)^{-1}\mathbf{z}_{l_{k_w}s_{k_w}}},\quad t=2,\ldots,N_t \tag{39}$$

while the original estimation is

$$\hat{\mathbf{M}}_{RMLE_k}(1) = \frac{N}{W}\sum_{w=1}^{W}\frac{\mathbf{z}_{l_{k_w}s_{k_w}}\mathbf{z}^H_{l_{k_w}s_{k_w}}}{\mathbf{z}^H_{l_{k_w}s_{k_w}}\mathbf{z}_{l_{k_w}s_{k_w}}} \tag{40}$$

with $N_t = 4$ [21].

Finally, the CFAR properties of three strategies of covariance matrix estimation are evaluated. The adaptive MSDs with SCM estimation strategy have an independent relationship with Gaussian clutter, yet dependent on the texture component in compound-Gaussian environment. Although in the compound-Gaussian background, the MSDs with NSCM estimation strategy are independent of the texture component for considering the normalization factor, they still depend on the structure of $\mathbf{M}$ [31]. And it has been proved that the RMLE is independent of both texture component and $\mathbf{M}$ [32].

4. SIMULATION

This section is devoted to the performance assessment on the adaptive MSDs based on the GLRT, Rao and Wald tests with different $\mathbf{M}$ estimators, SCM, NSCM and RMLE ($\mathbf{M}$-SCM, $\mathbf{M}$-NSCM, $\mathbf{M}$-RMLE in simulation). Assuming that the speckle component of the generated clutter data has an exponential correlation structure covariance matrix, hence $\mathbf{M}$ can be expressed as

$$[\mathbf{M}]_{N_iN_j} = \rho^{|N_i-N_j|},\quad 1 \le N_i, N_j \le N \tag{41}$$

where ρ is the one-lag correlation coefficient. Additionally, the target is set as Swerling 0 or Swerling 1 [33], usually encountered in various real conditions.

Since the closed-form expressions for both the P_{fa} and the probability of detection (P_d) are not available, we resort to standard Monte Carlo technique. More precisely, in order to evaluate the threshold necessary to ensure a preassigned value of P_{fa} and to

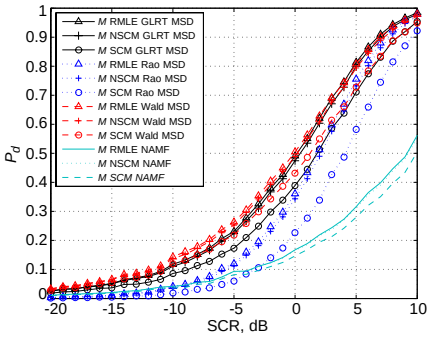

Figure 2. P_d versus SCR for 60 rpm, $N = 10$, $K = 4$, $\nu = 0.6$, $\rho = 0.9$, $W = 40$, and Swerling 0 target.

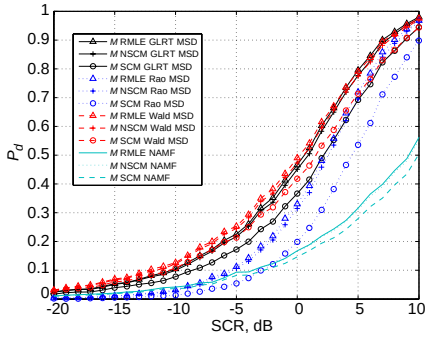

Figure 3. P_d versus SCR for 60 rpm, $N = 10$, $K = 4$, $\nu = 0.6$, $\rho = 0.9$, $W = 40$, and Swerling 1 target.

compute P_d, we resort to $100/P_{fa}$ and 10^6 independent trials, respectively.

Moreover, since laking of the sufficient multiple-scan real data, we resort to the simulation data, where the known steering vector is given by $\mathbf{p}_{l_k s_k} = [1, \exp(j2\pi f_{l_k s_k}), \ldots, \exp\big(j2\pi(N-1)f_{l_k s_k}\big)]^T$ with $j = \sqrt{-1}$ to match the condition when the normalized Doppler frequency f_d of the moving target is 0.8, i.e., $f_{l_k s_k} = f_d = 0.8$, and all simulations refer to the data parameters of a coherent X-band Enhanced Surveillance Radar [19] with a hypothetical 3° azimuth beamwidth antenna scanning at different rates, PRF = 750 Hz, and multiple scans, are combined over the integration time of 5 s with the unit power of the clutter in every scan.

The Signal-to-Clutter Ratio (SCR) is defined as

$$\mathrm{SCR} = \sum_{k=1}^{K} |a_{l_k s_k}|^2 \mathbf{p}_{l_k s_k}^H \mathbf{M}^{-1} \mathbf{p}_{l_k s_k} \tag{42}$$

In the first case, we consider the scenario: 60 rpm, $N = 10$, $K = 4$, $\nu = 0.6$, $\rho = 0.9$, and $W = 40$. The detection performance of MSD based on two-step GLRT (GLRT-MSD), Rao test (Rao-MSD) or Wald test (Wald-MSD) is compared with that of the traditional single-scan detector (NAMF). Figures 2 and 3 show the probability of detection curves versus SCR for Swerling 0 target and Swerling 1 target, respectively. Considering the correlation lengths of the texture component and speckle component, the data can be potentially deemed as statistically independent in reality [34].

As can be observed in Figure 2 and Figure 3, the performance

of both Wald-MSD and GLRT-MSD is better than that of the single-scan detector. The Rao-MSD with RMLE or NSCM estimator also outperforms NAMF when SCR > -8 dB. The discrepancy of detection performance is even more obvious as the value of SCR increases. In brief, the results clearly show that the adaptive MSDs exhibit the performance advantages over the single-scan processor.

In multiple-scan detection comparison, the performance of detectors with RMLE is superior to that with SCM estimator and slightly better than that with NSCM estimator. Additionally, both the Wald-MSD and GLRT-MSD show the better performance than the Rao-MSD whether the estimator $\mathbf{M}$ is.

In more general condition, when the RCS of the small target is Rayleigh-distributed across multiple scans, the detection curves shown in Figure 3 exhibit quite close to the results in Figure 2. It indicates that the fluctuating RCS of the target has little influence on multiple-scan detection. Similarly, all MSDs with RMLE strategy, shown in Figure 3, perform relatively well among the three estimators, almost as the same as the results in Figure 2. In summary, the comparison of detection curves reveals the similar superiority of MSDs under the two conditions (Swerling 0 and Swerling 1) in heavy compound-Gaussian clutter.

In the second case, to aim at researching the influence of scan rate on the multiple-scan detection performance in the same processing time (5 s), we consider another scenario of less scan-to-scan integrations (30 rpm) than that in the first case (60 rpm). Unlike the condition of 60 rpm ($N = 10$ and $K = 4$), though there are not straightforward parameters for 30 rpm presented in [19], according to the existing data parameters, we can be capable of setting the reasonable and available parameters: the value of N is 20 and the number of K is 2 where the other parameters are unchanged ($\nu = 0.6$, $\rho = 0.9$, and $W = 40$).

Obviously, in the single scan detection, it can be anticipated that the performance of all the algorithms will improve as the number of CPI increases due to the greater integrations with sufficient secondary data. However, in the multiple-scan detection, although the scanning radar can achieve more scan-to-scan integrations as the scan rate increases in a given integration period, there is an associated decrease in the number of pulse-to-pulse integrations within the dwell time of the antenna beamwidth. Consequently, considering the interplay of the CPI (pulse-to-pulse) and the scan rate (scan-to-scan) in the same time (5 s), we investigate the detection performance discrepancy of MSDs when the scan rate changes from 60 rpm to 30 rpm.

According to the results in Figures 2 and 3, the MSDs provide approximate detection performance for different target models. Hence,

for the purpose of conciseness, we only show the curves of the probability of detection for Swerling 0 target in Figure 4, and the results illustrate the serious performance degradation in the presence of slower scan rate. This can be explained by the fact that the effective multiple-scan detection is dependent on the coherence of the target signature. Hence, when the CPI increases from 10 to 20 pulses, there is a greater chance that the target Doppler will vary from the determinate targeted frequency $f_{l_k s_k}$ in the known steering vector, resulting in the detection performance loss [19]. Moreover, the poorer frequency selectivity maybe also offset by the greater number of scan-to-scan integrations.

In the third case, turning our attention to the detection performance of MSDs under the distinct clutter conditions, shown in Figure 5, the curves depict the detection performance variation when the shape parameter changes ($\nu = 0.4$ and $\nu = 0.6$). Additionally, the target is set as Swerling 1 while the correlation coefficient of clutter is $\rho = 0.9$, and the radar parameters are 60 rpm, $N = 10$ and $K = 4$ with $W = 40$. The results in Figure 5 show that all the MSDs with RMLE or NSCM estimator have better detection performance when the shape parameter decreases.

Moreover, when the shape parameter is equal to infinity, the K-distribution reduces to a Rayleigh distribution in amplitude, and on the contrary, it can be seen that the smaller ν is, the greater difference between K-distribution and Rayleigh distribution presents [12]. Additionally, U.S. Naval Research Laboratory does research on different sea-state scenarios using the HR X-band radar

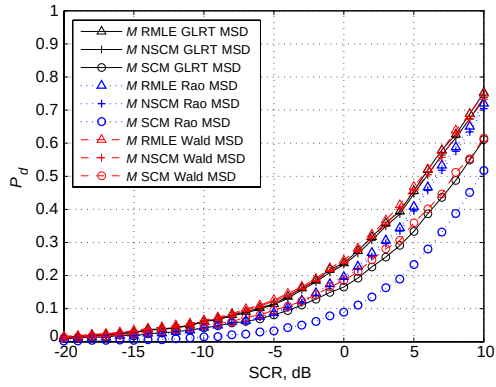

Figure 4. P_d versus SCR for 30 rpm, $N = 20$, $K = 2$, $\nu = 0.6$, $\rho = 0.9$, $W = 40$, and Swerling 0 target.

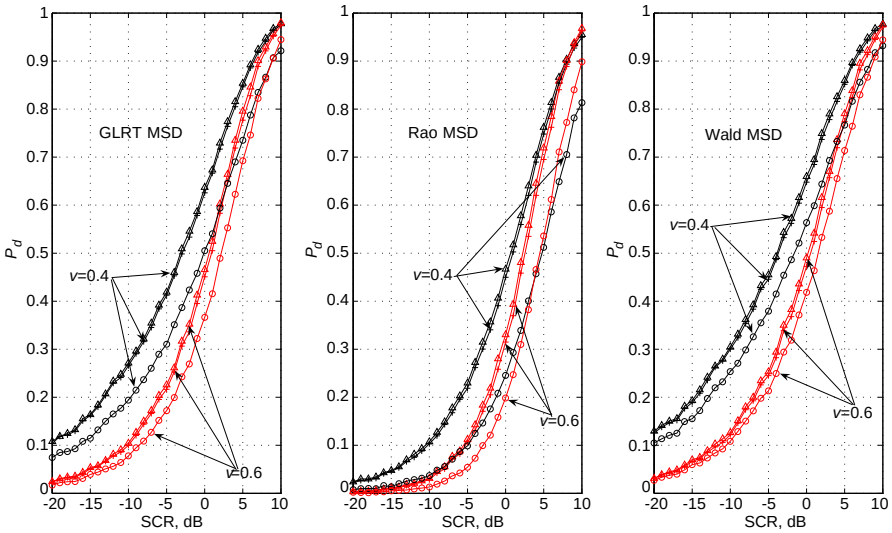

Figure 5. P_ds of GLRT-MSD, Rao-MSD and Wald-MSD versus SCR, for 60 rpm, $N = 10$, $K = 4$, $\rho = 0.9$, $W = 40$, and Swerling 1 target with different νs ($\nu = 0.4$ and $\nu = 0.6$); MSDs with SCM estimator: circle marker and solid line; MSDs with NSCM estimator: cross marker and solid line; MSDs with RMLE: triangle marker and solid line.

with vertical polarization and 0.5° beamwidth antenna in 1967. The observed results indicate that the higher sea-state is, the farther the distribution of sea clutter deviates from Rayleigh distribution.

Hence, the comparison results shown in Figure 5 declare that the adaptive MSDs, specially GLRT-MSD and Wald-MSD, are even more effective in relatively high sea-state scenario regardless of Swerling 0 (not shown in the paper) or Swerling 1 target. Clearly, when ν increases, the complex clutter in the paper gradually approximates to the complex Gaussian clutter. Therefore, it can be noticed that the clutter with $\nu = 0.6$ more tends to the complex Gaussian clutter compared to that with $\nu = 0.4$. Meanwhile, considering the effect of the texture nonexistent in the complex Gaussian clutter, the adaptive MSDs are derived on the basis of the compound-Gaussian background, and thereby they suffer some performance loss when it is closer to the complex Gaussian clutter. In additional, the MSDs with SCM estimator show the worse performance, indicating that the SCM estimator is indeed not appropriate for the compound-Gaussian clutter as discussed before.

In the last case, it is focused on the impact of the correlation

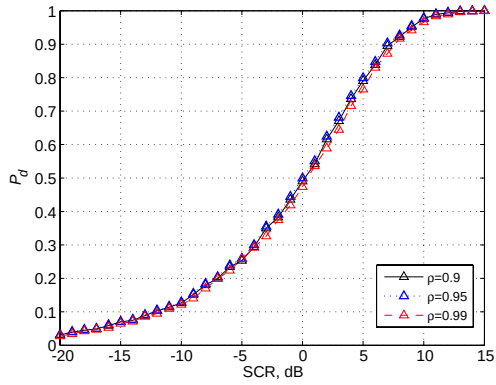

Figure 6. P_d of Wald-MSD based upon RMLE versus SCR for 60 rpm, $N = 10$, $K = 4$, $\nu = 0.6$, $W = 40$, and Swerling 1 target with different ρs.

coefficient on the detection performance. Observing that the typical values for radar sea clutter are in the range [0.9, 0.99] [21], hence, we consider the scenario: $N = 10$, $K = 4$, 60 rpm, $\nu = 0.6$, $W = 40$ and Swerling 1 target with various ρs. When the correlation coefficient varies, the detection performance of Wald-MSD with RMLE in Figure 6, or the other MSDs with it (not reported here), is almost unchanged. These MSDs are completely insensitive to the fluctuation in the value of ρ, presenting the robustness to the correlation property of the sea clutter.

In fact, it is straightforwardly seen that the model of the clutter is mainly determined by the shape parameter and the correlation coefficient. Therefore, combining the four cases, the adaptive MSDs with RMLE achieve the higher detectability than the conventional single-scan detector for the small target under the various conditions of sea clutter.

5. CONCLUSION

In this paper, we present the derivations of MSDs and analyze the detection performance of MSDs for the small RCS target embedded in the heavy sea clutter illuminated by the HR radar system. In HR radar scenario, the sea clutter is generally modeled as compound-Gaussian distribution described as SIRP. In the heavy clutter, the performance of single-scan detectors degrades, and hence the optimum MSD based on NP criterion is presented. Precisely, the NP criterion is resorted to derive the nonadaptive detector under the assumptions for known

clutter covariance matrix $\mathbf{M}$, the texture component $\tau_{l_k s_k}$ and the parameter $a_{l_k s_k}$. However, the prior knowledge of $\mathbf{M}$, $\tau_{l_k s_k}$ or $a_{l_k s_k}$ is commonly absent in the realistic environment. Consequently, for the purpose of overcoming this drawback, the adaptive MSDs based on the two-step GLRT, Rao and Wald tests are proposed, and three methods are used to estimate the unknown PSD.

Finally, Monte Carlo simulation results show that the adaptive MSDs significantly outperform the traditional single-scan detector for different targets. Obviously, the MSDs can availably reduce the effect of clutter outlier in a single scan, and also allow the target to be detectable with the smaller values of SCR across multiple scans. Additionally, the MSDs can attain more training data even in the heterogeneous scenarios where it is difficult to obtain enough secondary data in single-scan detection. Meanwhile, the results show that the performance of MSDs with RMLE is superior to that of MSDs with SCM or NSCM estimator in various backgrounds of sea clutter.

ACKNOWLEDGMENT

This work is sponsored by the National Natural Science Foundation of China (61178068) and by Sichuan Youth Science and Technology Foundation (2011JQ0024).

REFERENCES

1. Hatam, M., A. Sheikhi, and M. A. Masnadi-Shirazi, "Target detection in pulse-train MIMO radars applying ICA algorithms," *Progress In Electromagnetics Research*, Vol. 122, 413–435, 2012.
2. Qu, Y., G. S. Liao, S. Q. Zhu, and X. Y. Liu, "Pattern synthesis of planar antenna array via convex optimization for airborne forward looking radar," *Progress In Electromagnetics Research*, Vol. 84, 1–10, 2008.
3. Qu, Y., G. S. Liao, S. Q. Zhu, X. Y. Liu, and H. Jiang, "Performance analysis of beamforming for MIMO radar," *Progress In Electromagnetics Research*, Vol. 84, 123–134, 2008.
4. Sabry, R. and P. W. Vachon, "Advanced polarimetric synthetic aperture radar (SAR) and electro-optical (EO) data fusion through unified coherent formulation of the scattered EM field," *Progress In Electromagnetics Research*, Vol. 84, 189–203, 2008.
5. Herselman, P. L. and H. J. de Wind, "Improved covariance matrix estimation in spectrally inhomogeneous sea clutter with

application to adaptive small boat detection," *International Conference on Radar*, 94–99, 2008.

6. Lerro, D. and Y. Bar-Shalom, "Interacting multiple model tracking with target amplitude feature," *IEEE Transactions on Aerospace and Electronic Systems*, Vol. 29, No. 2, 494–509, 1993.
7. Rutten, M. G., N. J. Gordon, and S. Maskell, "Recursive track-before-detect with target amplitude fluctuations," *IEE Proceeding on Radar, Sonar and Navigation*, Vol. 152, No. 5, 345–352, 2005.
8. Ward, K. D., J. A. Tough, and S. Watts, "Sea clutter: Scattering, the k-distribution and radar performance," *IET Radar, Sonar and Navigation Series*, Vol. 20, 45–95, 2006.
9. Haykin, S., R. Bakker, and B. W. Currie, "Uncovering nonlinear dynamics-the case study of sea clutter," *Proceedings of the IEEE*, Vol. 90, No. 5, 860–881, 2002.
10. Unsworth, C. P., M. R. Cowper, S. McLaughlin, and B. Mulgrew, "Re-examining the nature of radar sea clutter," *IEE Processing on Rader Signal Processing*, Vol. 149, No. 3, 105–114, 2002.
11. Farina, A., F. Gini, M. V. Greco, and L. Verrazzani, "High resolution sea clutter data: Statistical analysis of recorded live data," *IEE Processing on Rader Signal Processing*, Vol. 144, No. 3, 121–130, 1997.
12. Nohara, T. J. and S. Haykin, "Canadian East Coast radar trials and the K-distribution," *IEE Processing on Rader Signal Processing*, Vol. 138, No. 2, 80–88, 1991.
13. Conte, E., A. De Maio, and C. Galdi, "Statistical analysis of real clutter at different range resolutions," *IEEE Transactions on Aerospace and Electronic Systems*, Vol. 40, No. 3, 903–918, 2004.
14. Greco, M., F. Bordoni, and F. Gini, "X-band sea-clutter nonstationarity: Influence of long waves," *IEEE Journal of Oceanic Engineering*, Vol. 29, No. 2, 269–293, 2004.
15. Greco, M., F. Gini, and M. Rangaswamy, "Non-stationarity analysis of real X-band clutter data at different resolutions," *IEEE National Radar Conference*, 44–50, 2006.
16. Ward, K. D., C. J. Baker, and S. Watts, "Maritime surveillance radar. I. Radar scattering from the ocean surface," *IEE Proceedings F on Radar and Signal Processing*, Vol. 137, No. 2, 51–62, 1990.
17. Panagopoulos, S. and J. J. Soraghan, "Small-target detection in sea clutter," *IEEE Transactions on Geoscience and Remote Sensing*, Vol. 42, No. 7, 1355–1361, 2004.
18. Schleher, D. C., "Periscope detection radar," *Record of the IEEE*

International Radar Conference, 704–707, 1995.

19. McDonald, M. and S. Lycett, "Fast versus slow scan radar operation for coherent small target detection in sea clutter," *IEE Proceedings on Radar, Sonar and Navigation*, Vol. 152, No. 6, 429–435, 2005.
20. Carretero-Moya, J., J. Gismero-Menoyo, A. Asensio-López, and Á. Blanco-del-Campo, "Application of the Radon transform to detect small-targets in sea clutter," *IET Radar, Sonar and Navigation*, Vol. 3, No. 2, 155–166, 2009.
21. Gini, F. and M. Greco, "Covariance matrix estimation for CFAR detection in correlated heavy tailed clutter," *Signal Processing*, Vol. 82, No. 12, 1847–1859, 2002.
22. Gini, F. amd A. Farina, "Vector subspace detection in compound-Gaussian clutter, Part I: Survey and new results," *IEEE Transactions on Aerospace and Electronic Systems*, Vol. 38, No. 4, 1295–1311, 2002.
23. Gini, F. and M. Greco, "Suboptimum approach for adaptive coherent radar detection in compound-Gaussian clutter," *IEEE Transactions on Aerospace and Electronic Systems*, Vol. 35, No. 3, 1095–1104, 1999.
24. Conte, E., A. De Maio, and G. Ricci, "Asymptotically optimum radar detection in compound Gaussian clutter," *IEEE Transactions on Aerospace and Electronic Systems*, Vol. 31, No. 2, 617–625, 1995.
25. Wang, P., H. Li, and B. Himed, "Parametric Rao tests for multichannel adaptive detection in partially homogeneous environment," *IEEE Transactions on Aerospace and Electronic Systems*, Vol. 47, No. 3, 1850–1862, 2011.
26. De Maio, A., S. M. Kay, and A. Farina, "On the invariance, coincidence, and statistical equivalence of the GLRT, Rao test, and Wald test," *IEEE Transactions on Signal Processing*, Vol. 58, No. 4, 1967–1979, 2010.
27. De Maio, A. and S. Iommelli, "Coincidence of the Rao test, Wald test, and GLRT in partially homogeneous environment," *IEEE Signal Processing Letter*, Vol. 15, 385–388, 2008.
28. Sangston, K. J. and K. R. Gerlach, "Coherent detection of radar targets in a non-gaussian background," *IEEE Transactions on Aerospace and Electronic Systems*, Vol. 30, No. 2, 330–340, 1994.
29. Anastassopoulous, V., G. A. Lampropoulos, A. Drosopoulos, and M. Rey, "High resolution radar clutter statistics," *IEEE Transactions on Aerospace and Electronic Systems*, Vol. 35, No. 1,

43–60, 1999.

30. Gini, F., G. B. Giannakis, M. Greco, and G. T. Zhou, "Time-averaged subspace methods for radar clutter texture retrieval," *IEEE Transactions on Signal Processing*, Vol. 49, No. 9, 1896–1898, 2001.
31. Gini, F., "Performance analysis of two structured covariance matrix estimators in compound-Gaussian clutter," *Signal Processing*, Vol. 80, No. 2, 365–371, 2000.
32. Pascal, F., Y. Chitour, P. Forster, and P. Larzabal, "Covariance structure maximum-likelihood estimates in compound Gaussian noise: Existence and algorithm analysis," *IEEE Transactions on Signal Processing*, Vol. 56, No. 1, 34–48, 2008.
33. Swerling, P., "Radar probability of detection for some additional fluctuating target cases," *IEEE Transactions on Aerospace and Electronic Systems*, Vol. 33, No. 2, 698–709, 1997.
34. Güntürkün, U., "Toward the development of radar scene analyzer for cognitive radar," *IEEE Journal of Oceanic Engineering*, Vol. 35, No. 2, 303–313, 2010.